*Research Article*

# Combined Influence of Particle Shape and Fabric on the Shear Behaviour of Granular Materials

**Yuan-Yuan Liu,[1,2] Yaping Zhang,[3] Yanrong Li ⓘ,[3] and Yi-Chen Guo[1]**

[1]*Department of Civil Engineering, Faculty of Building Engineering, North China Institute of Science and Technology, Sanhe 100044, Hebei, China*
[2]*Hebei Provincial Key Laboratory of Civil Engineering Catastrophe Control and Disaster Emergency Response, North China Institute of Science and Technology, Sanhe 100044, Hebei, China*
[3]*Department of Earth Sciences and Engineering, Taiyuan University of Technology, Taiyuan 030024, Shanxi, China*

Correspondence should be addressed to Yanrong Li; li.dennis@hotmail.com

The anisotropy feature is an important characteristic of granular materials in natural life and is caused by two facts: the anisotropy feature of particle shape, such as an elongated or flattened shape, and the anisotropy feature of the packing fabric, such as the preferable orientation of particle alignment. The discrete element method has been commonly used in the study of meso-mechanics of granular materials and is in our study to simulate the direct shear test with particles of various aspect ratios under different initial orientation alignment conditions for assessing the coupled influence of anisotropy from particle shape and fabric of particle packings on the shear behaviour of granular materials. Analysis results show that anisotropy from the particle shape has the most significant influence on the shear behaviour of a granular packing when the packing has the initial anisotropy fabric of an orientational alignment perpendicular to the shear direction. Moreover, the initial fabric anisotropy of a granular packing has an increasing influence with the rise in anisotropy of particle shape. A combined anisotropic factor is finally introduced to reflect the coupled influence of the shape anisotropy of particles and the fabric anisotropy of particle packings.

## 1. Introduction

Particles of natural granular materials have mostly non-rounded shapes and are arranged in various fabric patterns in real life. For example, the preferred direction of the long axis of particles is horizontal when the cohesionless soil with elongated or flattened particles deposits under gravity, and this condition would lead to the anisotropy feature of the deposited soil. Anisotropy is an important feature and imposes a notable influence on the mechanical behaviour of granular packings, which has been attracting much research interest in the field of powder and soil engineering [1–6].

Anisotropy of granular materials comes from not only the anisotropy of particle shape, such as elongated or flattened particles, but also the anisotropy of fabric in particle packings, such as the preferable orientation of particle alignment. One conventional shape descriptor for the shape anisotropy feature is aspect ratio [7, 8], which is the ratio of the length over the width of a particle. The influence of aspect ratio on the shear behaviour of granular materials has been investigated in previous studies [1–3, 8–10]. The results show that the shear strength of granular assemblies would be strongly enhanced with the increase in aspect ratio due to the possible attribution of a better ability of the elongated particles to interlock [1, 2, 8, 10, 11]. The solid fraction [2, 11], the contact number [2, 3], the prevailing contact type [2, 12], and the critical state [9] were also found to be relevant to the aspect ratio. In the meantime, the initial packing geometry is another important influencing factor of mechanical behaviour [6, 13], and other works focused on the influence of the initial anisotropy characteristic of a

granular packing, that is, the initial orientation alignment of nonrounded particles, on the macromechanical and micromechanical behaviour [4, 5, 11]. The shear behaviour of samples with different initial particle orientations is significantly different. For example, the specimen with a vertical orientation has a higher shear strength but a smaller coordination number than the specimens with random and horizontal orientation [4].

However, some questions still need to be answered. For example, which of the shape anisotropy of particles and the fabric anisotropy of packings is more critical to determine the anisotropy feature for materials needs to be determined given that they have influence on the shear behaviour of granular materials. Moreover, it is unclear whether a granular packing with particles of a higher respect ratio value has absolutely higher shear strength than that of a lower respect ratio value, regardless of the initial orientational alignment of the particles. So far, few relevant works look into the coupled influence of the shape anisotropy of particles and the fabric anisotropy of particle packings on the anisotropy behaviour of granular materials, which is worthy of being explored.

The direct shear test has the advantage of a simple setup [14, 15], and the discrete element method (DEM) is a powerful method to perform virtual mechanical testing of granular materials [16–19].

In this study, we aim to explore the response of a series of granular systems of elongated particles with different respect ratios under various initial orientational alignments in the direct shear test with the help of DEM owing to its simplicity. For this purpose, we use clumps in DEM to simulate rounded and elongated particles with a respect ratio of 1 to 3, and we also generate elongated particles in assemblies under three initial alignment orientations: random, perpendicular, and parallel to the shear direction. Notably, possible particle breakage resulting from shearing has been verified to also obviously affect the mechanical properties of granular material [17, 18]. However, the influence from particle breakage is ignored in this study to focus on the combined influence of particle shape and particle initial packing pattern.

## 2. Test Programme

*2.1. Sample Preparation.* In this research, numerical simulations were conducted on uniformly graded rounded and elongated particles with different aspect ratios under various initial orientational alignments using PFC2D (Particle Flow Code in 2 Dimensions; Itasca, 2004 [20]).

*2.1.1. Particle Shape.* Elongated particles were modelled as a juxtaposition of two or more disks of radius $R$ with the total length $L$ and width $W$ (Figure 1). The aspect ratio $AR = L/W$ increases from 1.0 with one circle disk up to 3.0 with three jointed circle disks. As shown in Table 1, the generated samples were represented as I–IV with the corresponding respect ratios of particle shape of 1.0, 1.25, 2.0, and 3.0, respectively.

The initial void ratio, initial density, and particle size grading were set at the same level for all samples for the direct shear testing to focus on the effect of respect ratio of particle shape on the mechanical features. For this purpose, we adopted the equivalent area and density principles. The area of an elongated cluster can be expressed with the area of each clustered circle disk, as shown in equation (1). With the equivalent area principle, the areas of particles in all samples should be the same, that is, the area of cluster in each sample should be equal to the disk area of sample I, as expressed in equation (2).

$$S_{\text{cluster}} = \sum S_{\text{diskincluster}} - S_{\text{overlap}}, \tag{1}$$

$$S_{\text{clusterinsamples}} = S_{\text{diskinsample}\,I}. \tag{2}$$

From equation (2), the radius of the disk used in the cluster of sample II with an aspect ratio of 1.25 (Figure 2) can be expressed with the radius of the circular particle of sample I as follows:

$$R_{II} = 0.871R_I. \tag{3}$$

Similarly, the radii of the circular particles used in the elongated clusters of the rest samples are obtained as follows:

$$R_{\text{III}} = 0.707R_I, R_{\text{IV}} = 0.577R_I. \tag{4}$$

The equivalent density principle is adopted here to keep the same initial densities for all samples. The equivalent density is expressed as the ratio of the total mass and the equivalent area of clusters in samples II–IV. Given that the equivalent area of the clusters in samples I–IV is equal to each other, the total mass of each sample should be the same. In PFC, the total mass is equal to the product of the density and exact area of the disks used in the elongated clusters in samples II–IV or the circle disks in sample I. As a result, the input value of the exact density of disk used in the elongated clusters in samples II–IV can be obtained as an equation.

$$P_{\text{II,IIIorIV}} = \frac{A_I}{\sum A_{\text{II,IIIorIV}}} \rho_I, \tag{5}$$

where $\rho_I$ and $A_I$ are the density and area of circular disk of sample I, respectively. $P_{\text{II,IIIorIV}}$ and $A_{\text{II,IIIorIV}}$ are the density and area of circular particle used in the elongated cluster of samples II–IV.

*2.1.2. Alignment of Particles.* The alignment of particles is defined as the direction of the long axis of the particle and can be expressed as the angle between the long axis of the particle and the horizontal direction. Particles of each sample were generated under three orientational alignments, namely, (a) horizontal direction, (b) random direction, and (c) vertical direction, as shown in Figure 1, to investigate the influence of initial particle alignment on the shear behaviour of granular materials with different particle shapes.

*2.1.3. Preparation of Specimens.* A total of 15 specimens were prepared with the same initial situations by combining the five particle shapes and three initial alignments
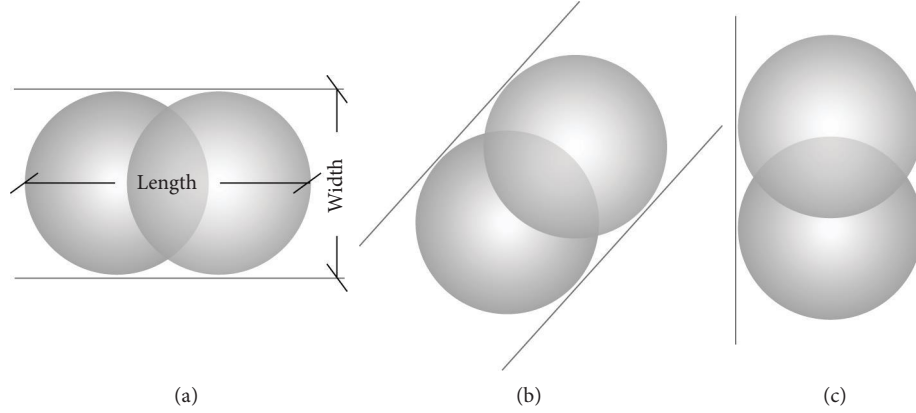
FIGURE 1: Three initial alignments of particles in specimens: (a) horizontal alignment; (b) random alignment; (c) vertical alignment.

TABLE 1: Shape parameters of particles used for sample preparation.

| Particle | I | II | III | IV |
|---|---|---|---|---|
| Shape | | | | |
| Aspect ratio (L/W) | 1 | 1.25 | 2 | 3 |

above into the simulation. The parameters adopted in the model of sample I with round particles are listed in Table 2 as the baseline values. For all samples, the initial porosity $e_0$ is 0.4 and the initial density $\rho_0$ is 1.89 g/cm$^3$. The sizes of disks in sample I were distributed between 0.6 and 2 mm, as shown in Figure 3, and the relative unit weight was set as 2650 N/m$^3$. The linear contact model with normal stiffness $K_n$ and tangent stiffness $K_s$ has been commonly considered in considerable previous research to investigate the mechanical behaviour of granular material and is used here [21]. Referring to previous calibration studies on biaxial test simulation [22, 23], the normal stiffness $K_n$ and tangential stiffness $K_s$ of particles were set to be 20 and 10 MPa, respectively, whilst the normal stiffness $K_n$ and tangential stiffness $K_s$ of walls were set to be 2000 and 0 MPa to simulate rigid boundaries. The friction coefficient was set at 0.5 between particles and 0 MPa between particle and wall.

The shear box was modelled by walls in simulation, as illustrated in Figure 4. The size of the shear box was set at 50 mm square and 30 mm height. The lower part of the shear box was modelled by walls 1, 2, 3, and 4; the upper part was modelled by walls 4, 5, 6, and 7. The purpose of walls 7 and 8 was to avoid the outflow of particles from the ends of the shear zone during the process of shearing. The walls were regarded as rigid in their normal direction, and their surface was smooth. Thus, the normal stiffness of walls was 2000 MPa and the friction coefficient of walls was set to 0.

*2.2. Testing Process.* After generation was completed, a sample was firstly consolidated one-dimensionally under the designed consolidation vertical stress of $\sigma_v = 100$ kPa. Then, it was sheared in the horizontal direction under a quasi-static condition.
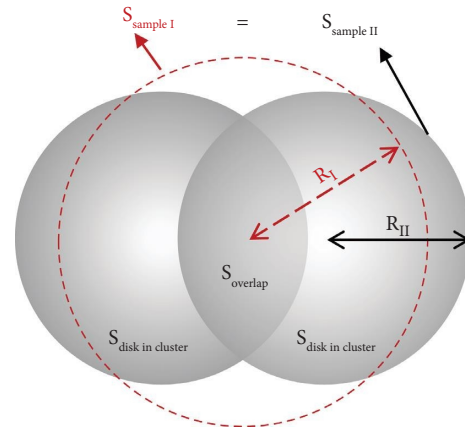


FIGURE 2: Sketch of the equivalent area principle for samples II and I. $S_{diskincluster}$ and $R_{II}$ are the area and radius of each disk used in the elongated cluster of sample II. $S_0$ is the overlap area of circular disks in the elongated cluster of sample II. $S_{sampleII}$ is the area of cluster in sample II. $S_{sampleI}$ and $R_I$ are the area and radius of disk in sample I.

The consolidation process was modelled in PFC2D by the upper covering wall (wall 5) moving downwards with a controlled velocity until the vertical consolidation stress $\sigma$ between particles and the wall reached the designed consolidation stress value of 100 kPa. The distance of the downward movement of the covering wall was regarded as the consolidation displacement. The consolidation process was regarded as complete once this wall cannot move further with the vertical stress $\sigma_v$ being 100 kPa and the consolidation displacement remaining constant.

After consolidation was completed, the shearing force was loaded by the lower part of the shear box, which is a movable part that moves horizontally in the right direction at a constant speed. The target of choosing a suitable shear speed value was to keep the shearing process quasi-static. No exact relationship was considered between the shearing speed value used in physical experiments and that adopted in DEM simulation. In previous studies [11, 14, 23–25], the shearing speed value ranged widely from 0.0006 mm/s to 0.1 mm/s. The influence of the shear speed on the mechanical behaviour of cohesionless materials was also insignificant

TABLE 2: Parameters adopted in modelling of sample I as baseline values.

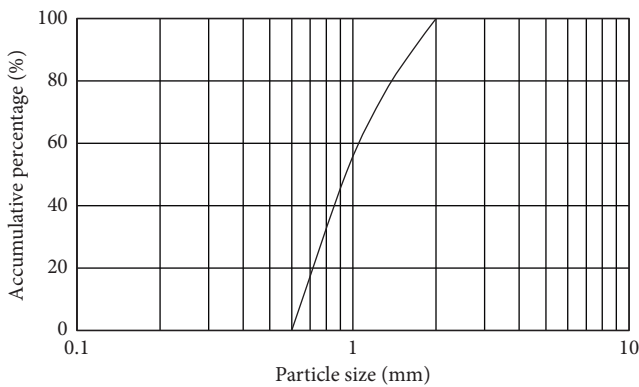| Unit | Parameter | Value |
| --- | --- | --- |
| Particles | Number | 918 |
| | Specific gravity (N/m$^3$) | 2650 |
| | Particle size range (mm) | 0.6–2 |
| | Normal stiffness, kn (MPa) | 20 |
| | Shear stiffness, ks (MPa) | 10 |
| | Basic friction | 0.5 |
| Walls | Normal stiffness, kn (MPa) | 2000 |
| | Shear stiffness, ks (MPa) | 0 |
| | Friction | 0 |
| Initial situation | Porosity, $e_0$ | 0.4 |
| | Density, $\rho_0$ (g/cm$^3$) | 1.89 |



FIGURE 3: Particle size grading curve of specimen.



FIGURE 4: Shearing box model.

under the quasi-static situation, especially before the material reached its peak value. We set the shear speed to be 0.01 m/s with comprehensive consideration of time efficiency and reasonable accuracy. The shear stress $\tau$ and the corresponding shear strain $\varepsilon$ were monitored during the shearing process. The shearing process was stopped when the shear strain was over 15%. The vertical stress $\sigma_v$ was kept constant by a servo control algorithm during the whole shearing process.

## 3. DEM Simulation Results

In this section, samples with different respect ratios under three initial alignments were compared to analyse the consolidation displacement, void ratio change, angular distribution probability density change during consolidation process and peak and residual stress values, angular distribution, void ratio change, and contact force map change during shearing process.

### 3.1. Change in Vertical Displacement and Void Ratio during Consolidation. 
Rearrangement of particles under the vertical consolidation stress causes consolidation displacement and changes in the void ratio. Figure 5 shows the vertical consolidation displacement curve developing with the time step for the specimens with different respect ratios under three initial alignment conditions. For each consolidation
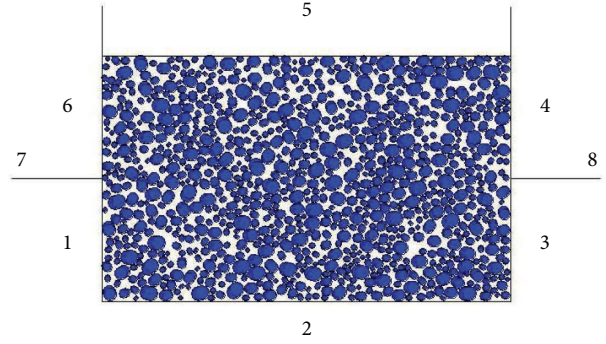
process, the vertical displacement increases with each time step and finally approaches a constant value. Spatial positions of particles would be rearranged and trends to compress to each other under the consolidation loading. The corresponding void ratios after consolidation for all specimens with different aspect ratios and under different initial alignment conditions are also plotted in Figure 6.

Comparing the consolidation curves with different aspect ratios under the same initial alignment shows that the final consolidation displacement generally decreases when particles become increasingly elongated. The void ratio after consolidation generally increases with the increment in aspect ratio under the same initial alignment. These trends indicate that the elongated particles with higher aspect ratios would hinder themselves from sliding and rotating towards each other. For elongated particles, three types of contact exist between two elongated particles: cap-to-cap, cap-to-side, and side-to-side [2]. When the particle shape is close to round, the major contact type is cap-to-cap; rotating over each other is easy, and the packing is easy to be compressed to a denser status. With the increase in respect ratio of particles, the contact network would be mostly dominated by the complex contacts of cap-to-side and side-to-side, both of which can accommodate force chains that are usually unsustainable by cap-to-cap contacts [2]. These formed force chains benefit local arching structures appearing with much void space and prevention of particles further moving to each other under the vertical consolidation force.

Comparing the void ratios of specimens with the same aspect ratio but under different initial alignments indicates that the difference in the void ratio after consolidation caused by different initial alignments increases with the increment in aspect ratio, as shown in Figure 6. Particles with an initial alignment parallel to the loading direction (vertical alignment here) is easier to compress to a denser packing with a lower final packing porosity than that of perpendicular direction (horizontal alignment here).

### 3.2. Change in Particle Alignment after Consolidation. 
Figure 7 illustrates the angular distribution probability densities of the long axis of particles in specimens with particle aspect ratios of 1.25, 2, and 3 under three initial alignment conditions. When the particle alignment direction is horizontal (perpendicular to the consolidated force
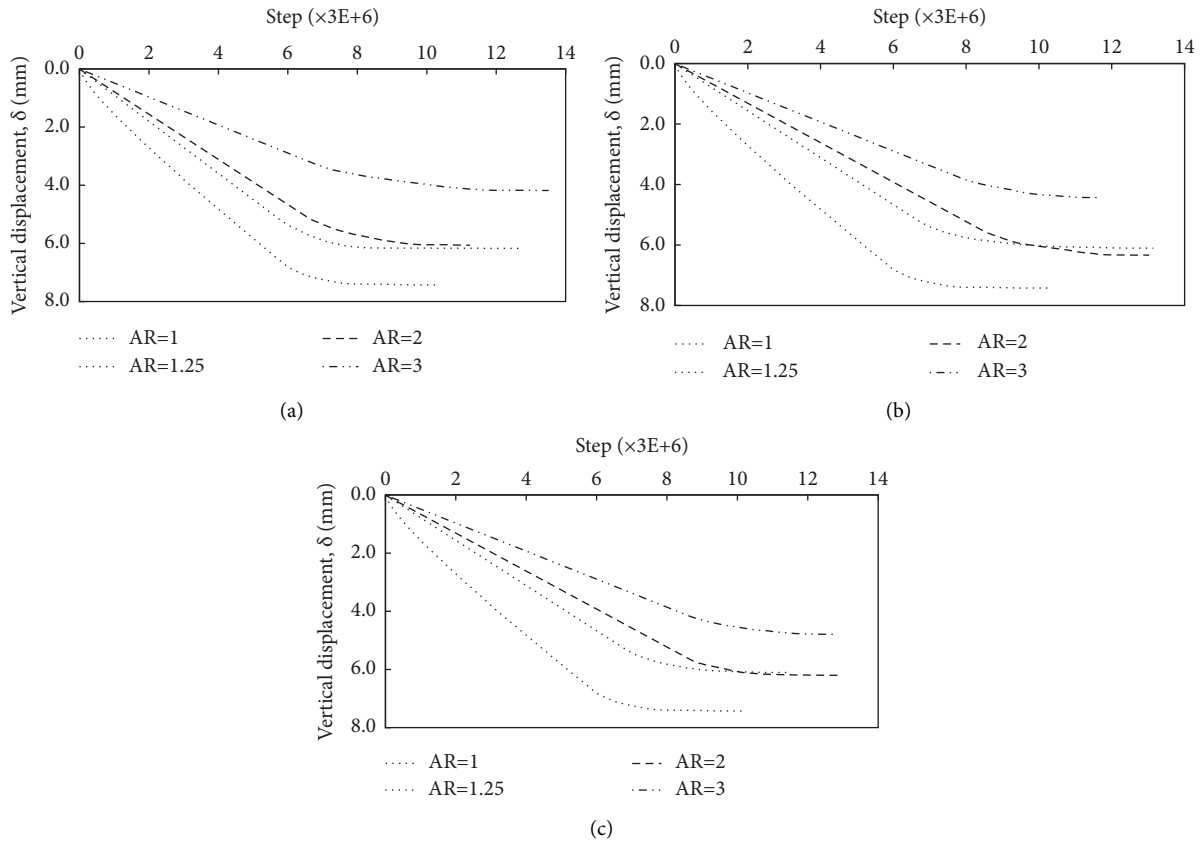
Figure 5: Consolidation displacement of specimens with different particle aspect ratios of 1.0, 1.25, 2.0, and 3.0 under three initial alignments: (a) horizontal, (b) random, and (c) vertical.
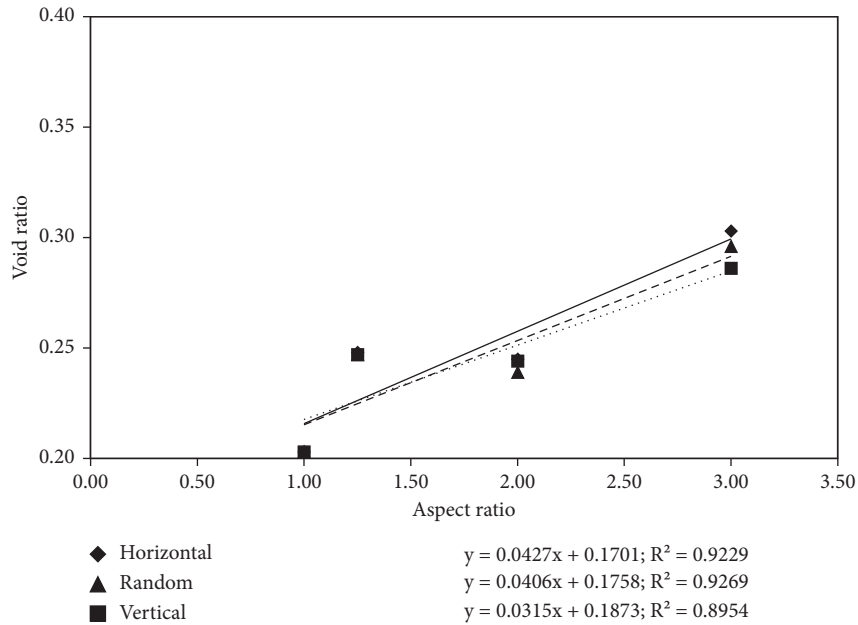


Figure 6: Void ratio of specimens after consolidation with aspect ratios under different initial alignments.

direction), as shown in Figure 7(a), and the respect ratio is 1.25, the density of the angular direction around 0° and 180° is slightly reduced, and the reduced part is mostly shifted to that around 90° and 270°. When the respect ratio increases,

the density distribution shows no obvious change after consolidation. This finding indicates that the particles for specimens with the horizontal initial alignment would mostly move downwards without much rotation under the
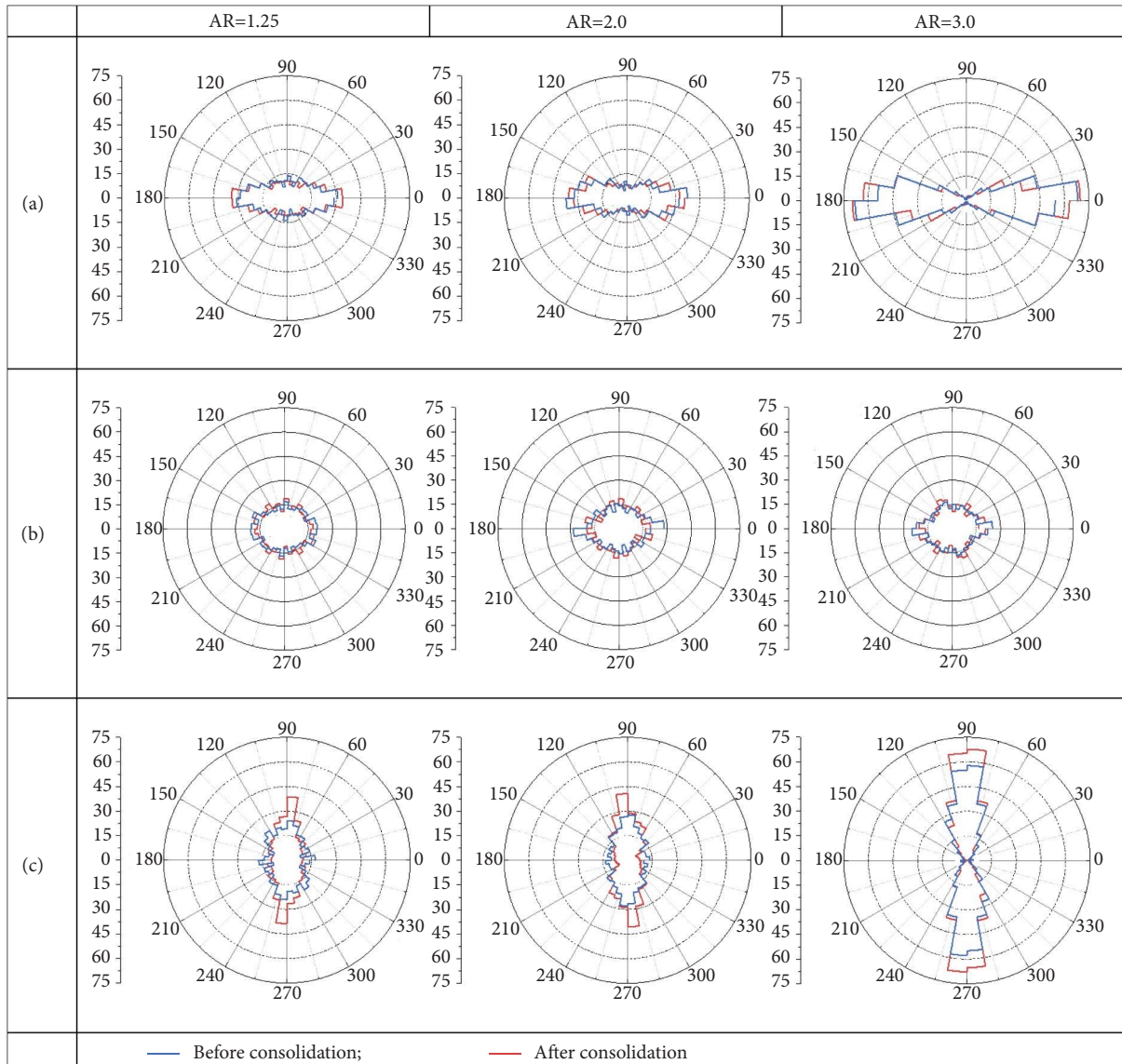
FIGURE 7: Angular distribution probability densities (%) of the long axis of particles in specimens with different alignments before and after consolidation.

vertical consolidation force, especially for more elongated particles with a higher respect ratio value. When the initial direction of particle alignment is random, as shown in Figure 7(b), the angular distribution probability density of the long axis of particles would generally change from a uniform distribution pattern before consolidation to a slightly anisotropy distribution pattern with a major horizontal direction after consolidation. The change appears more obvious for the specimens with a larger respect ratio. When the initial direction of particle alignment is vertical (parallel with the consolidation force direction), as shown in Figure 7(c), the density of angular distribution around 90° is obviously reduced after consolidation, and this reduction is always obvious regardless of the aspect ratio.

The abovementioned comparison shows that the level of angular distribution density in the vertical direction would be kept for the specimens with a horizontal initial alignment and reduced for the specimens with a random or vertical initial alignment after consolidation. That is, the initial alignment situation would cause different effects on the revolution of the anisotropy feature of particle arrangement during consolidation: the anisotropy is kept under a horizontal initial alignment condition, strengthened under a random initial alignment condition, and weakened under a vertical initial alignment. The increasing aspect ratio of particle shape would weaken the reduction due to the difficulty of rotation over each other for more elongated particles with easier interlocking appearing.

### 3.3. Stress-Strain Relationship during Shearing. The shear stress-strain curves of all specimens under the same vertical stress of 100 kPa are plotted in Figures 8 and 9 to illustrate the influence of particle shape and the initial alignment condition. Each plot in Figure 8 shows the developing curves of shear stress with the increase in shear strain for specimens
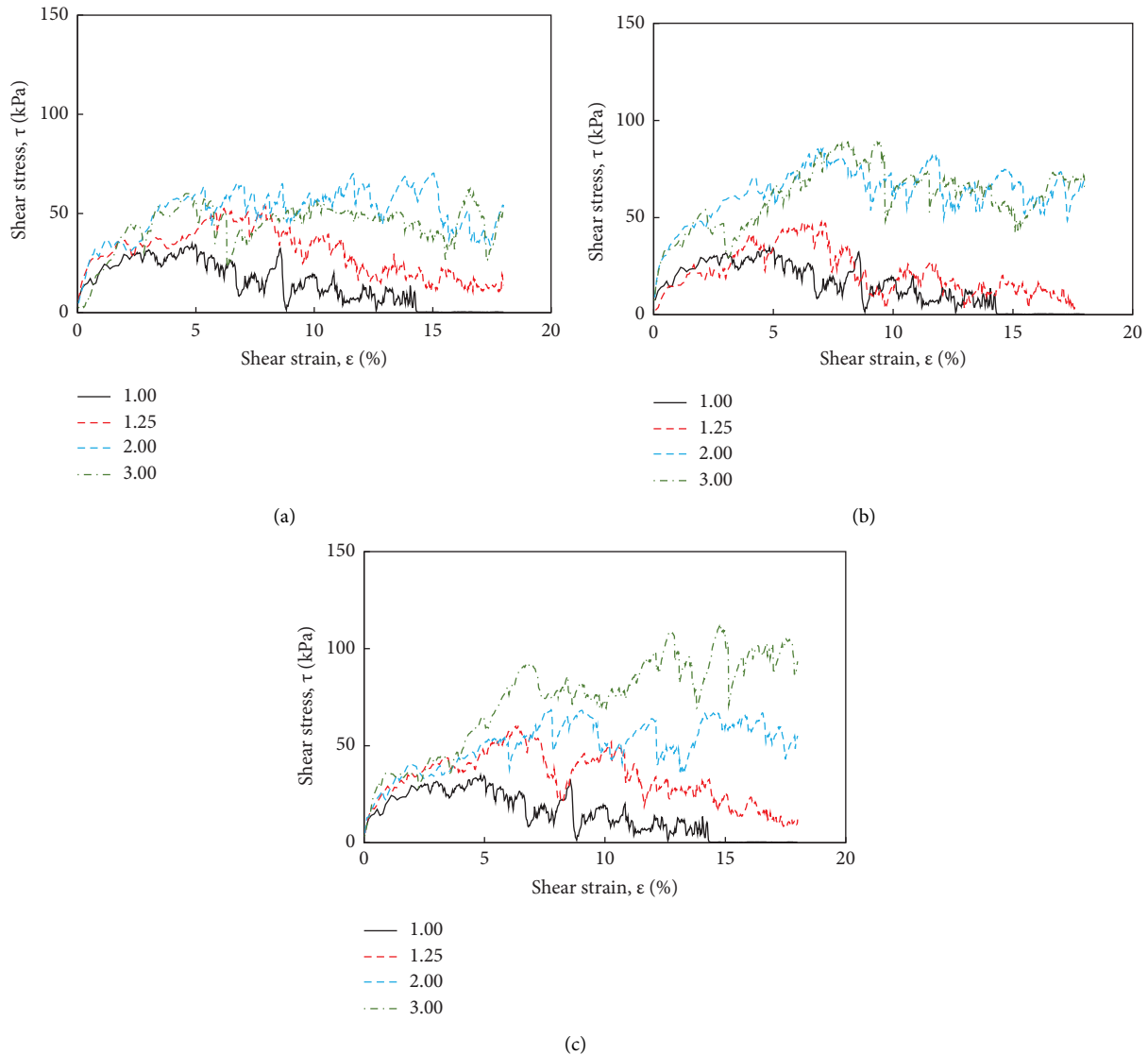
FIGURE 8: Shear stress-strain curves of specimens with different particle shapes under the vertical stress of 100 kPa during the shearing process under three initial alignment conditions: (a) horizontal, (b) random, and (c) vertical.

with different aspect ratios of particle shape under the same initial alignment. Under the horizontal alignment condition, as plotted in Figure 8(a), the shear stress generally occurs slightly higher for specimens with higher aspect ratios than for those with lower aspect ratios. In the starting stage, with the shear strain being lower than 3%, the shear stress increases with the development of shear strain, and the difference in these curves appears to be negligible. After the shear strain reaches 3%, a more obvious difference appears amongst these stress-strain curves for different particle shapes: the shear stress reaches the peak level and then decreases to a constant level with the development in shear strain when the aspect ratios are smaller, such as 1 and 1.25; the shear stress continuously increases until approaching a constant level without the occurrence of a peak value during the whole shearing process when the aspect ratios are larger, such as 2 or 3. Figures 8(b) and 8(c) compare the stress-strain curves of specimen of various particle shapes under

the random and vertical initial alignment conditions, respectively. The developing trends of curves under the random and vertical initial alignment conditions generally agree with those in the abovementioned case of horizontal initial alignment. However, the difference in stress-strain curves of different aspect ratios of particle shape, especially in the case of vertical initial alignment in Figure 8(c), is much larger than the difference in curves in the case of horizontal initial alignment in Figure 8(a). This finding illustrates that the aspect ratio of particle shape may affect the shear stress of granular materials regardless of the initial alignment. The corresponding stress would also be increased with the rise in respect ratio for the same strain, which has already been well agreed upon in previous studies. However, the intensity of the effect of the aspect ratio is highly influenced by the initial alignment condition, which has not been mentioned in previous studies so far. The effect of aspect ratio is most significant in the case of vertical initial alignment, least

significant in the case of horizontal initial alignment, and between the former two in the case of random initial alignment.

Figure 9 compresses the shear stress-shear strain curves of specimens with the same aspect ratio under three initial alignment conditions, namely, horizontal, random and vertical. The difference in stress-strain curves amongst three initial alignment cases is not obvious in specimens with the respect ratios of 1.25 and 2, as shown in Figures 9(a) and 9(b). However, the gap amongst the curves under three alignment conditions becomes significantly larger when the aspect ratio is increased to 3, as shown in Figure 9(c). The curve of specimen under the vertical initial alignment is the highest and the curve of specimen under the horizontal initial alignment is the lowest. The curve of specimen under the random initial alignment is between those of the former two. Therefore, the initial alignment direction imposes significant effect on the shear behaviour of granular material only when the aspect ratio is sufficiently higher, that is, for highly elongated particles.

As shown in Figures 8(c) and 9(c), the shear stress has even exceeded 100 kPa when the aspect ratio is 3 under the vertical initial alignment. One of the possible reasons of such high stress level is the strong interlocking amongst highly elongated particles when the shearing direction is perpendicular to the particle alignment, and the material strength of particles is stirred to contribute to the shear stress of the whole assembly of particles. Another possible reason may be that the rotation of the shearing surface due to the dilatancy easily occurs in the sample with highly elongated particles when the shearing direction is perpendicular to the particle alignment. This occurrence leads to a higher apparent shear stress measured in the direct shear test.

As shown in Figures 8 and 9, the shear stress-strain curves fluctuate, especially in the later stage. In fact, fluctuations of shear stress and vertical displacement with shear displacement have been observed during laboratory tests and numerical simulations of granular materials [26–28]. The magnitude of the fluctuation was reported to correlate to the intrinsic properties of materials, such as the particle size distribution, the particle-particle friction, and the degree of irregularity of the shear surface [28]. Figures 8 and 9 show that the elongation of particle shape imposes a greater influence on the magnitude of stress fluctuation than the initial particle alignment. The fluctuation in the stress-strain curve becomes more obvious with the increase in aspect ratio. The reason could be that particles with a higher aspect ratio are easier to interlock and need more energy to climb over each other temporarily.

### 3.4. Peak and Residual Stress Values.
Figure 10 summarises the peak and residual strengths of each specimen. The peak and residual values of shear stress generally increase with the rise in the aspect ratio of particle shape, regardless of the initial alignment. Moreover, the effect of the aspect ratio on the peak and residual shear stress is most obvious for the specimens under the vertical initial alignment, and it is the least obvious for the specimens under the horizontal initial alignment. In the meantime, the effect of different initial alignment conditions increases with the rise in aspect ratio. In general, the specimen under the initial vertical alignment has the highest peak and residual values, and that under the initial horizontal alignment has the lowest ones with the same aspect ratio.

### 3.5. Particle Alignment Evolution during Shear.
Figure 11 illustrates the evolution of the angular distribution probability densities during the shearing process (with shear displacements of 1, 3, and 5 mm, corresponding to shear strains of 0.02%, 6%, and 10%, respectively) for the specimens with particles of various respect ratios under different initial particle alignments. In general, the change in particle alignment orientation during the shearing process is not obvious with horizontal alignment. However, the probability density of the angular around 90° (i.e., the vertical direction) decreases, and that of the angular around 0° (i.e., the horizontal direction) increases in the horizontal and vertical initial alignment cases, especially when the particle shape is not much elongated. This result means that the rotation of particles occurs much more in the cases of random and vertical initial alignments than in the case of horizontal alignment and may cause higher shear stress during the shearing process, as shown in Figure 9. This rotational movement of particles is attributed to the strong force chains forming along the shearing direction under the vertical initial alignment.

The range of changing percentage before and after the shearing process is relatively larger for specimens with the vertical initial alignment, as shown in Figure 12. This finding indicates that the rotation movement occurs more in the specimen of vertical initial alignment under the horizontal shear loading than that in the specimens of horizontal and random initial alignments. For the specimens with the vertical initial alignment, the percentage of vertical particles with an angle of 60°–90° transfers to that of a horizontal particle of 0°–30° when the particle shape is lowly elongated, and to that of a declinate particle of 30°–60° when it is highly elongated. For the specimens with the horizontal initial alignment, the percentage of horizontal particles slightly transfers to the percentage of vertical particles when the particle shape is lowly elongated and to that of declinate particles when it is highly elongated. For the specimens with the random initial alignment, the change in particle direction is from declinate direction to horizontal direction when the particle shape is lowly elongated; no obvious change in particle direction occurs when the particle shape is highly elongated. All of the abovementioned results indicate that the shearing process may reduce the anisotropy feature for all particles in the specimen when the initial anisotropy of particle alignment is strong. In the meantime, the shearing process may increase the anisotropy feature of all particles when the initial anisotropy of particle alignment is low. Moreover, the elongation value of 0.5 is a significant milestone level, above which the consolidation and shearing behaviour of granular materials would be obviously affected by the initial alignment situation.
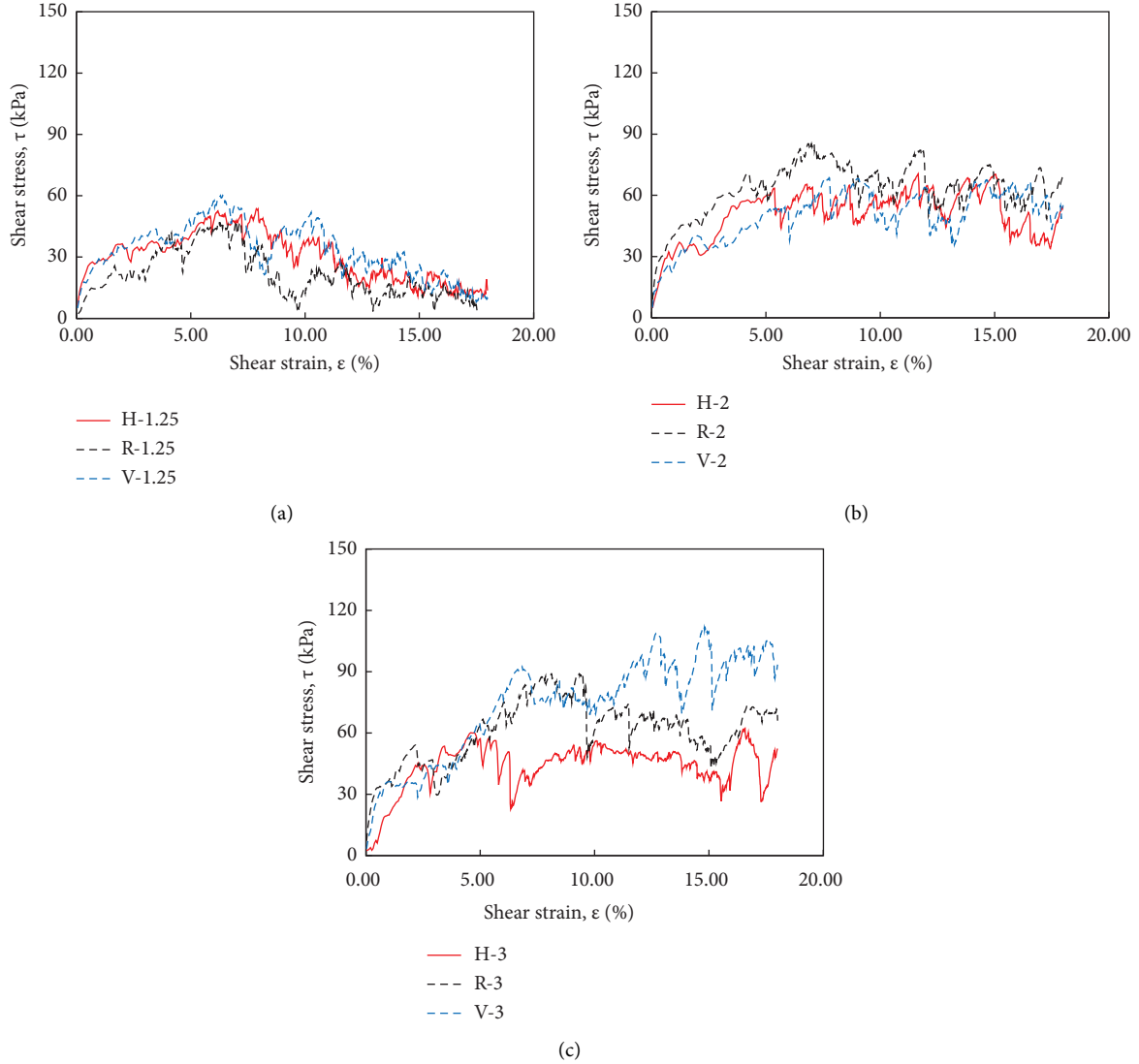
FIGURE 9: Comparison of shear stress of specimens with different initial particle alignments under the vertical stress of 100 kPa during the shearing process: (a) AR = 1.25; (b) AR = 2.0; (c) AR = 3.0.

## 4. Discussion

*4.1. Combined Anisotropic Factor.* The results in Section 4 indicate that the aspect ratio and the initial orientational alignment influence the shear behaviour, but the influences from the two factors are affected by each other. The reason is that the two factors are contributors to the fabric anisotropy feature of a granular material packing. We define a combined anisotropy factor (CAF) to determine the relationship between the fabric anisotropy feature and the shear behaviour. CAF may reflect the attribution based on the aspect ratio and the initial orientational alignment. It is expressed as

$$CAF = AR \times \left(\frac{\pi}{2} + \theta\right), \tag{6}$$

where AR is the value of the aspect ratio of the particle shape. $\theta$ is the radian value of the initial orientational alignment referring to the shear loading direction (the horizontal axis here). The radian values in this study are 0°, 45°, and 90° for the horizontal, random, and vertical alignments, respectively. The peak and residual values of shear stress for each specimen are plotted as functions of the CAF with the fitting curves, as shown in Figure 13. The fitting equations are listed as follows:

$y = 37.65e^{0.1244x}, R^2 = 0.8498$ are for the peak stress value.

$y = 10.806x - 7.2235, R^2 = 0.8527$ are for the residual stress value.

The general trends for the relationships between the peak and residual stress values monotonously increase with the rise in the CAF value. The fitting curve is given as an exponential curve for the peak value and a linear curve for the residual value, which indicates that the peak value of shear stress is more sensitive to the CAF value than the residual value of shear stress.
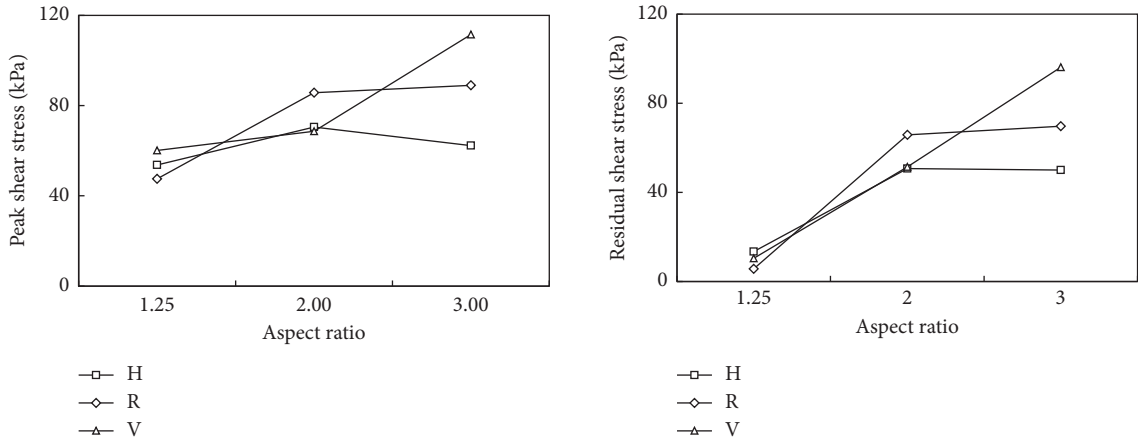
FIGURE 10: Peak and residual shear strengths with the increase in aspect ratio.
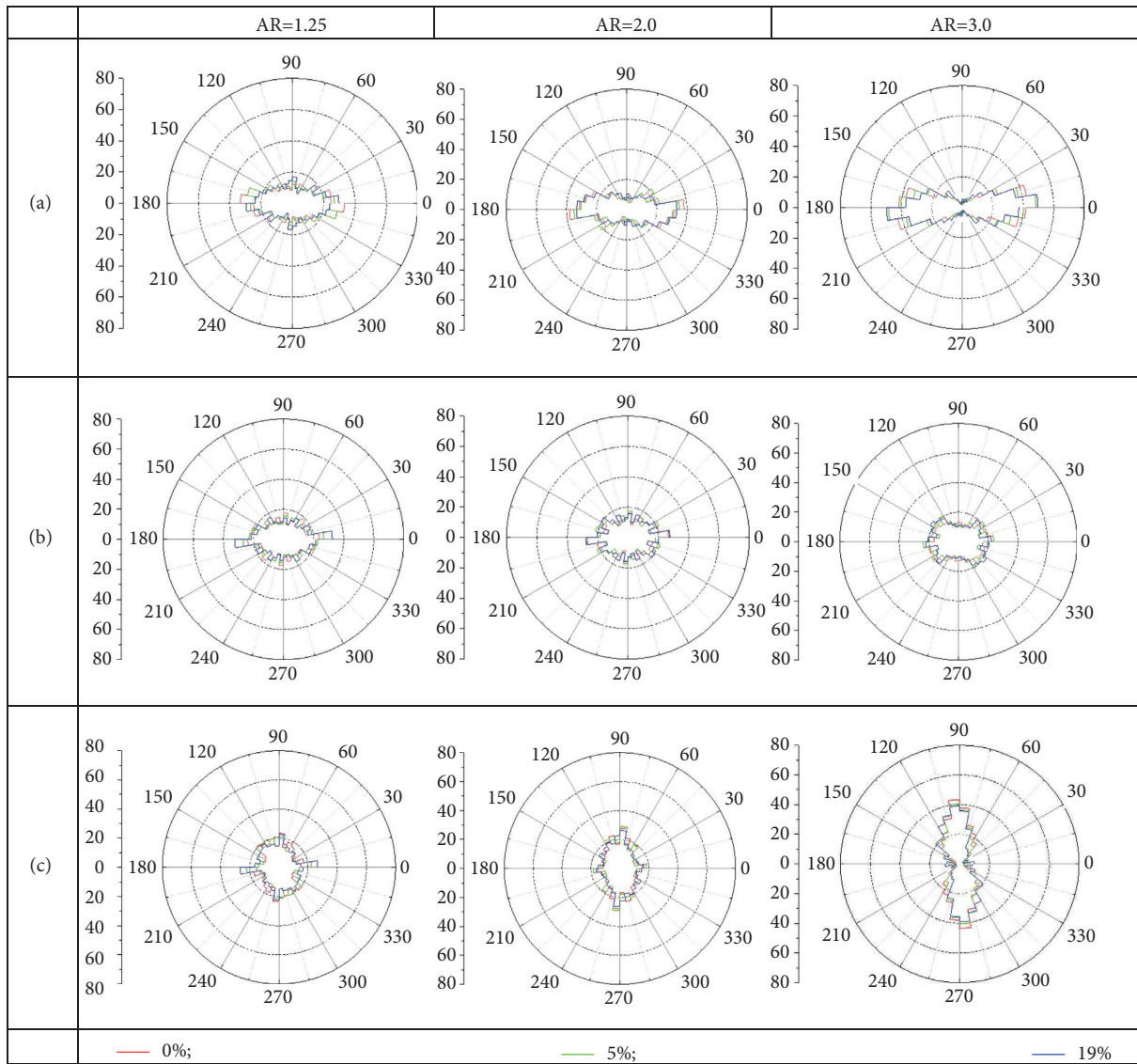


FIGURE 11: Probability density function (%) of the angular distribution of the long axis of particles in specimens with different initial particle alignments during shear process: (a) horizontal initial alignment; (b) random initial alignment; (c) vertical initial alignment.
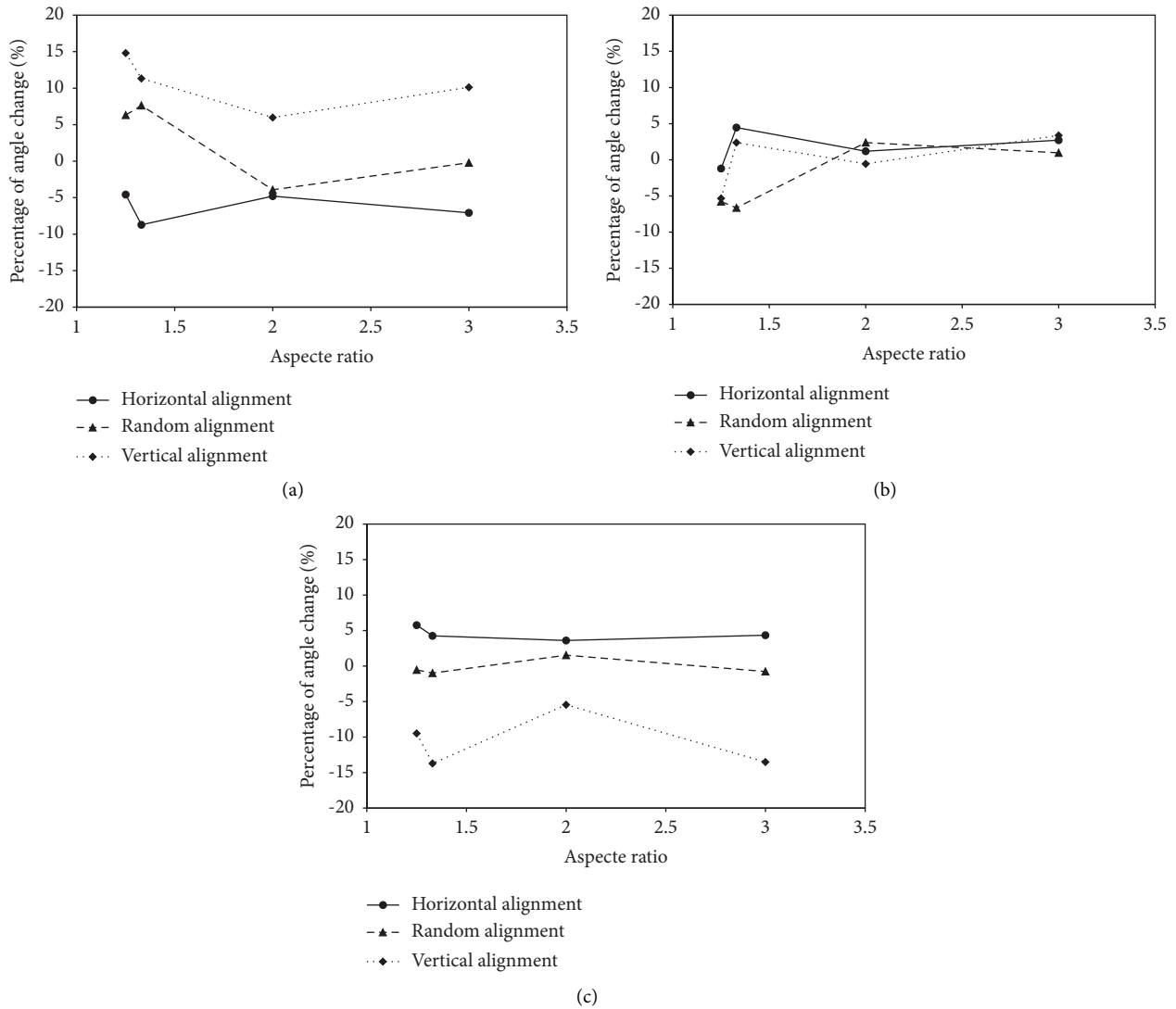
(a)



(b)



(c)

FIGURE 12: Percentage of angle change of the particle long axis to horizontal direction for specimens with various aspect ratios under three initial alignments before (shear strain of 0) and after shearing (shear strain of 19%) in the ranges of (a) 0°–30°, (b) 30°–60°, and (c) 60°–90°.
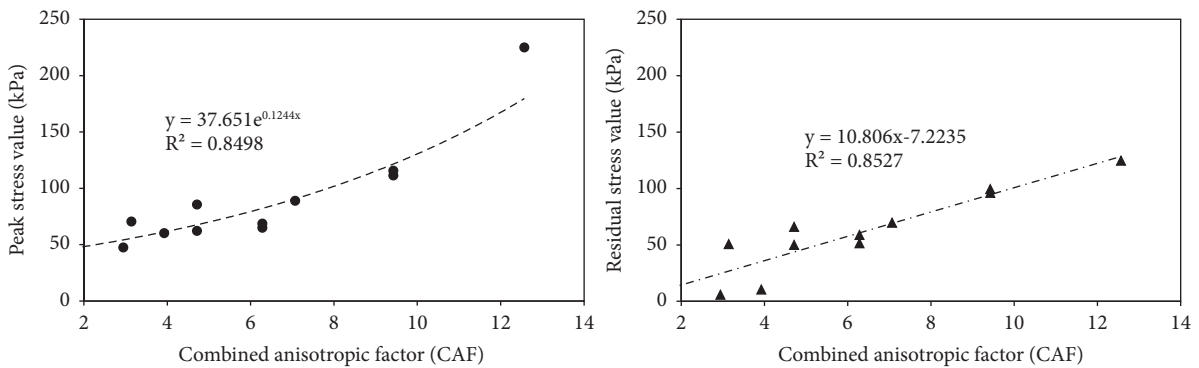


FIGURE 13: Peak and residual values vs. the combined anisotropic factor (CAF).

## 4.2. Force Chains during Shearing.

Figure 14 shows the strain-stress curves of four specimens with various CAF values and the development of force chain networks in these specimens. The stress level during the shearing is higher in the specimen with a higher CAF value, which agrees with the conclusion drawn in Section 4.1. The shear loading in a granular material assembly is transmitted from particle to particle through contact points. The normal and tangent
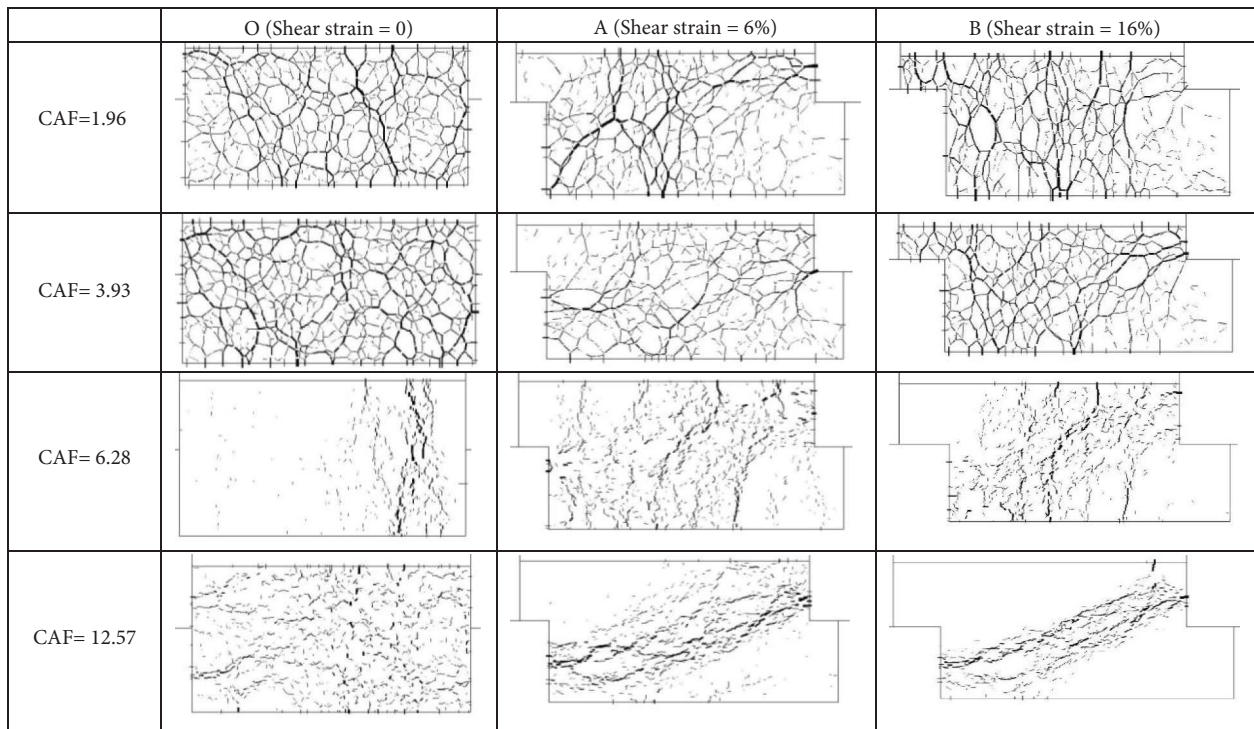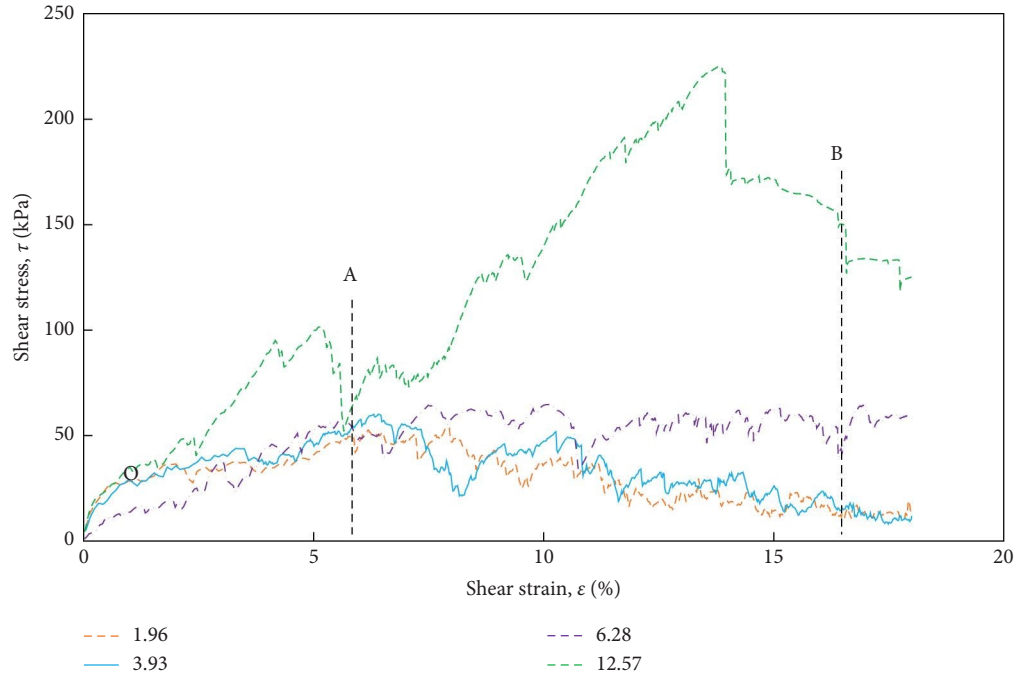
Figure 14: Contact force chains formed in specimens with different CAF values during shearing.

forces occurring at the contact points would develop mechanically stable and jammed contact networks during the shearing process to resist the loading [14], and the development of force chain networks may indicate the fabric evolution of granular assemblies and explain the origin of shear stress differing for specimens with different CAF values. The force networks are traced at three points: O, A, and B, with strains of 0%, 6%, and 16%, respectively (Figure 14). At the beginning point O, without any strain, the

force chains are mainly aligned with the vertical direction. The vertical load is translated to the particles that are in contact with the upper wall through the contact points. Then, it quickly spreads downwards, forming several main force chains. At a strain of 5%, the shear stress increases, and most contact force orientations rotate anticlockwise and form major force chains with the direction of the major principal stress. The shear stress occurring in the specimen is higher and the formed force chains are more distinguished
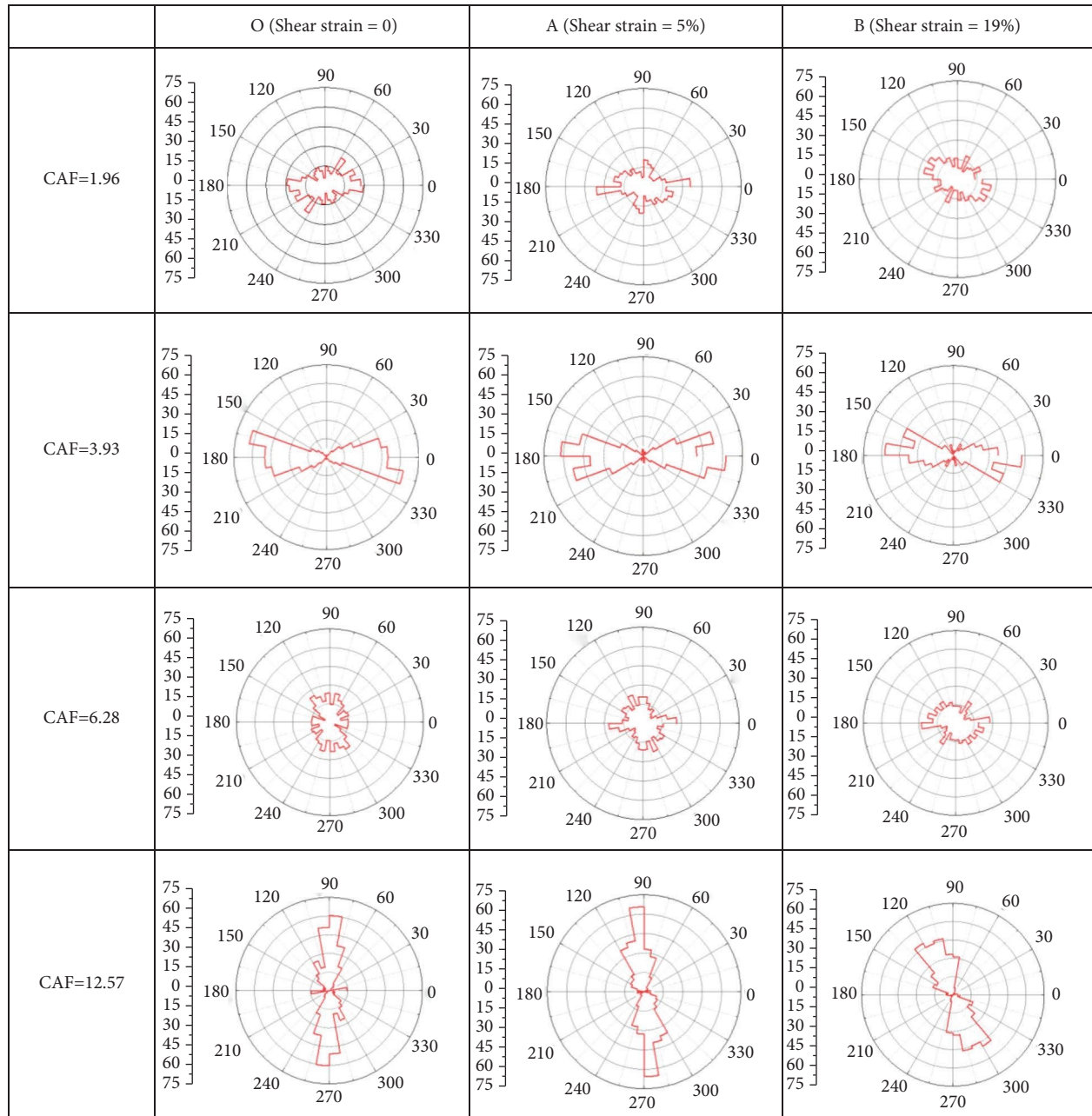
Figure 15: Probability density function (%) of angular distribution of the long axis of particles in specimens with different CAF values at the shear strains of 0% (point O), 5% (point A), and 19% (point B).

when the CAF value of the specimen is larger. At a shear strain of 10%, the shear stress level becomes lower than that of 5% for specimens with CAF values of 1.96 and 3.93, and the formed force chains recover to the vertical direction with less concentration. However, for specimens with CAF values of 6.28 and 12.57, the corresponding stress level to shear strain of 10% is greater than that of 5%, and the formed force chains remain aligned along the major principal stress and become more concentrated. The abovementioned comparison implies that the higher shear stress in specimens with a higher CFA value comes from the more concentrated force chains aligning with the direction of the major principal stress formed in the assembly.

4.3. Particle Alignments in Shearing Band Zone Evolution during Shearing. The magnitudes of the particle rotation inside and outside the shear band obviously differ [14]. The shear bands are defined as the zone with a width of 10 times the particle diameter beside the horizontal interface of the upper and lower parts of the testing box to capture the feature of the shear band indicated by particle rotation. Particles within the shear band zone are identified by recognising their $y$ positions, and the rotation of these particles is traced during the shearing process. Figure 15 shows the probability density functions of the long axis of particles within the shear band zones for the specimens with CFA values of 1.96, 3.93, 6.28, and 12.57 at points O, A, and B with

shear deformations of 0, 3, and 8 mm. Particles generally rotate in the shear band zone of all specimens. Comparing specimens with different particle respect ratio values under the same initial alignment situation shows that the more elongated particles with a larger aspect ratio rotate less than the less elongated particles with a lower aspect ratio within the shear band zone of the specimens. Comparing specimens with the same particle shape but under different initial alignment situations reveals that the particles in specimens under vertical alignment show more obvious rotation than those in specimens under horizontal alignment. Notably, the long axis direction of particles after rotation tends to be perpendicular to the corresponding force chain direction illustrated in Figure 14 during the shearing process. This observation indicates that the force chains during shearing to resist the horizontal shear loading are mostly provided by the side-to-side contact amongst particles, which agrees with the conclusion that the major contact type of elongated particles is side-to-side drawn in previous studies [2].

## 5. Conclusions

The coupled influence of the particle shape and initial alignment condition is investigated for 2D granular assemblies under direct shear tests. The DEM results of macroscopic and microscopic responses are analysed. We can then assert a few conclusions, as follows:

(1) The influence of respect ratio of particle shape on the consolidation and shear behaviour of granular assemblies is affected by the initial alignment condition. The influence of respect ratio in vertical and random initial alignments is much more obvious than that in horizontal initial alignment.

(2) The influence of the initial alignment condition on the consolidation and shear behaviour of granular assemblies is also affected by the respect ratio of particle shape. The influence of the initial alignment condition becomes increasingly obvious with the rise in respect ratio.

(3) A CAF of the shape anisotropy and the fabric anisotropy is defined in this study. A monotonously increasing relationship exists between the shear stress and the CAF value.

(4) The higher shear stress of specimens with a higher CAF value results from stronger force chains aligning with the major principal direction

This study also has some limitations that require future works. The shearing model in this study is simplified into a 2D situation with movements of particles only allowed within a plane, which is somewhat different from the actual 3D situation of the shear test. Some qualitative conclusions on the joint influence of particles and the initial alignment condition are provided here, and the validity of the 3D situation is expected to be further investigated with a 3D model in the future.

In the meantime, the numerical simulation in this study is conducted under a relatively low normal stress without considering particle crushing during the consolidation and shearing processes. The joint influence of particle shape and the initial alignment condition with consideration of particle crushing will be evaluated in the future to account for higher normal stress environments with high fidelity.

## Data Availability

The data that support the findings of this study are available from the corresponding author upon request.

## Conflicts of Interest

The authors declare that they have no conflicts of interest.

## Authors' Contributions

Yuan-Yuan Liu and Yaping Zhang contributed equally to this work.

## Acknowledgments

## References

[1] T. Borzsonyi and R. Stannarius, "Granular materials composed of shape-anisotropic grains," *Soft Matter*, vol. 9, no. 31, pp. 7401–7418, 2013.

[2] E. Azema and F. Radjai, "Stress-strain behavior and geometrical properties of packings of elongated particles," *Physical Review*, vol. 81, no. 5, Article ID 051304, 2010.

[3] D. Wang, H. Zheng, Y. Ji, J. Bares, and R. P. Behringer, "Shear of granular materials composed of ellipses," *Granular Matter*, vol. 22, no. 1, p. 5, 2020.

[4] A. A. Mirghasemi and M. Naeij, "The effect of initial elongation of elliptical particles on macro-micromechanical behavior during direct shear test," *Procedia Engineering*, vol. 102, pp. 1476–1483, 2015.

[5] H. Yang, W.-J. Xu, Q.-C. Sun, and Y. Feng, "Study on the meso-structure development in direct shear tests of a granular material," *Powder Technology*, vol. 314, pp. 129–139, 2017.

[6] C. O. R. Abbireddy and C. R. I. Clayton, "The impact of particle form on the packing and shear behaviour of some granular materials: an experimental study," *Granular Matter*, vol. 17, no. 4, pp. 427–438, 2015.

[7] M. L. Hentschel and N. W. Page, "Selection of descriptors for particle shape characterization," *Particle & Particle Systems Characterization*, vol. 20, no. 1, pp. 25–38, 2003.

[8] T.-T. Ng, W. Zhou, G. Ma, and X. L. Chang, "Macroscopic and microscopic behaviors of binary mixtures of different

particle shapes and particle sizes," *International Journal of Solids and Structures*, vol. 135, pp. 74–84, 2018.

[9] J. Yang and X. D. Luo, "Exploring the relationship between critical state and particle shape for granular materials," *Journal of the Mechanics and Physics of Solids*, vol. 84, pp. 196–213, 2015.

[10] Y. H. Xie, Z. X. Yang, D. Barreto, and M. D. Jiang, "The influence of particle geometry and the intermediate stress ratio on the shear behavior of granular materials," *Granular Matter*, vol. 19, no. 2, p. 35, 2017.

[11] J. Hartl and J. Y. Ooi, "Numerical investigation of particle shape and particle friction on limiting bulk friction in direct shear tests and comparison with experiments," *Powder Technology*, vol. 212, no. 1, pp. 231–239, 2011.

[12] Y. Yang, Y. M. Cheng, and J. A. Wang, "Exploring the contact types within mixtures of different shapes at the steady state by DEM," *Powder Technology*, vol. 301, pp. 440–448, 2016.

[13] B. B. Dai, J. Yang, C. Y. Zhou, and X. D. Luo, "DEM investigation on the effect of sample preparation on the shear behavior of granular soil," *Particuology*, vol. 25, pp. 111–121, 2016.

[14] M. J. Jiang, J. Liu, Z. Shen, and B. Xi, "Exploring the critical state properties and major principal stress rotation of sand in direct shear test using the distinct element method," *Granular Matter*, vol. 20, no. 2, p. 25, 2018.

[15] M. Nitka and A. Grabowski, "Shear band evolution phenomena in direct shear test modelled with DEM," *Powder Technology*, vol. 391, pp. 369–384, 2021.

[16] T. Qu, M. Wang, and Y. Feng, "Applicability of discrete element method with spherical and clumped particles for constitutive study of granular materials," *Journal of Rock Mechanics and Geotechnical Engineering*, vol. 14, no. 1, pp. 240–251, 2022.

[17] T. Wang, H. Huang, F. Zhang, and Y. Han, "DEM-continuum mechanics coupled modeling of slot-shaped breakout in high-porosity sandstone," *Tunnelling and Underground Space Technology*, vol. 98, Article ID 103348, 2020.

[18] F. Zhang, M. Li, M. Peng, C. Chen, and L. Zhang, "Three-dimensional DEM modeling of the stress–strain behavior for the gap-graded soils subjected to internal erosion," *Acta Geotechnica*, vol. 14, no. 2, pp. 487–503, 2018.

[19] Y. Zhu, J. Gong, and Z. Nie, "Shear behaviours of cohesionless mixed soils using the DEM: the influence of coarse particle shape," *Particuology*, vol. 55, pp. 151–165, 2021.

[20] Itasca, *User's Manual for PFC2D*, Itasca Consulting Group, Inc, Minneapolis, MN, USA, 2005.

[21] J. Gong, Z. Nie, Y. Zhu, Z. Liang, and X. Wang, "Exploring the effects of particle shape and content of fines on the shear behavior of sand-fines mixtures via the DEM," *Computers and Geotechnics*, vol. 106, pp. 161–176, 2019.

[22] I. R. Bezuijen, *Biaxial Test Simulations with PFC2D*, DelfracConsortium, Netherlands, Europe, 2002.

[23] L. Kong and R. Peng, "Particle flow simulation of influence of particle shape on mechanical properties of quasi-sands," *Chinese Journal of Rock Mechanics and Engineering*, vol. 10, pp. 2112–2119, 2011.

[24] M. Asadzadeh and A. Soroush, "Fundamental investigation of constant stress simple shear test using DEM," *Powder Technology*, vol. 292, pp. 129–139, 2016.

[25] S.-J. Feng, Y.-Q. Wang, and H.-X. Chen, "DEM simulation of geotextile-geomembrane interface direct shear test considering the interlocking and wearing processes," *Computers and Geotechnics*, vol. 148, Article ID 104805, 2022.

[26] Y. R. Li and A. Aydin, "Behavior of rounded granular materials in direct shear: mechanisms and quantification of fluctuations," *Engineering Geology*, vol. 115, no. 1-2, pp. 96–104, 2010.

[27] C. J. Coetzee, "Calibration of the discrete element method and the effect of particle shape," *Powder Technology*, vol. 297, pp. 50–70, 2016.

[28] S. Wang and Y. Huang, "Experimental study on the effect of particle size on the shear characteristics of large-displacement soil exposed to heat treatment: shear fluctuation and heat degradation," *Engineering Geology*, vol. 300, Article ID 106581, 2022.